RSC Advances

RSC Publishing

PAPER

View Article Online
View Journal | View Issue

Published on 15 July 2013. Downloaded by Pennsylvania State University on 18/09/2016 01:02:11.

Amidoxime porous polymers for CO_2 capture

Cite this: *RSC Advances*, 2013, **3**, 17203

Sonia Zulfiqar,[a] Sehrish Awan,[b] Ferdi Karadas,[c] Mert Atilhan,*[c] Cafer T. Yavuz*[d] and Muhammad Ilyas Sarwar*[b]

Received 16th May 2013,
Accepted 12th July 2013

DOI: 10.1039/c3ra42433b

www.rsc.org/advances

CO_2 capture from fossil fuel based electricity generation remains costly since new power plants with monoethanol amine (MEA) as the scrubbing agent are under construction. Amidoximes are known to mimic MEA, and porous polymers with amidoximes could offer a sustainable solution to carbon capture. Here we report the first amidoxime porous polymers (APPs) where aromatic polyamides (aramids) having amidoxime pendant groups were synthesized through low temperature condensation of 4,4′-oxydianiline (ODA) and *p*-phenylene diamine (*p*-PDA) with a new type of nitrile-bearing aromatic diacid chloride. The nitrile pendant groups of the polyamides were converted to an amidoxime functionality by a rapid hydroxylamine addition (APP-1 and APP-2). The CO_2 adsorption capacities of these polyamides were measured at low pressure (1 bar) and two different temperatures (273 and 298 K) and high pressure (up to 225 bar – the highest measuring pressure to date) at 318 K. The low pressure CO_2 uptake of APP-1 was found to be 0.32 mmol g^{-1} compared with APP-2 (0.07 mmol g^{-1}) at 273 K, whereas at high pressure they showed a substantial increase in CO_2 adsorption capacity exhibiting 24.69 and 11.67 mmol g^{-1} for APP-1 and APP-2 respectively. Both aramids were found to be solution processable, enabling membrane applications.

1. Introduction

Climate change is one of the most momentous issues confronted by humanity and society as a whole. The rise in global temperatures is expected to initiate a number of dire consequences, including rising sea levels, alteration in ecosystems, loss of biodiversity and diminution in crop yields.[1] Therefore, it is desirable to deploy defensive counter-steps against the imminent threat created by global warming. This alarming environmental situation has been attributed to an increasing dependence on the combustion of fossil fuels which accounts for anthropogenic greenhouse gas emissions.[2] However, at present there are no possible alternative energy sources to completely substitute mineral fuels. Accordingly, CO_2 capture and storage (CCS) is conceived as an integral and primary action to mitigate the environmental impacts due to escalating atmospheric CO_2 concentration. The conventional process employed for carbon dioxide capture is reversible solvent absorption but it possesses many limitations such as toxicity, degradability, high regeneration energy requirements and corrosive behavior.[3,4]

Adsorption is emerging as a superior technology for CO_2 capture with possible energy savings relative to other more established absorption processes.[5,6] Various solid sorbents have been explored as potential adsorbents for CO_2 capture. These include supported amines,[7–10] carbon-based sorbents,[11–18] supported carbonates,[19,20] hydrotalcites[21] and zeolites.[22–24] Unlike liquids, solid adsorbents can be used over a wider temperature range, produce less waste during cycling, and the exhausted material can be disposed of without excessive environmental precautions. These are also being exploited in pressure swing adsorption (PSA) systems for the purification of hydrogen in petrochemical industries.[25–27] The sequestered CO_2 can be used as a chemical raw material in the preparation of dry ice, carbonated beverage manufacturing,[28,29] dry cleaning processes[30] and in enhanced oil recovery (EOR) from oil wells, although the emissions are two orders of magnitude higher (32 000 Mton yr^{-1}) than the CO_2 market (250 Mton yr^{-1}).[31]

The interaction between CO_2 and N-containing organic heterocyclic molecules such as pyridine, imidazole and tetrazole has been investigated,[32] as their basic nitrogen atoms can bind to acidic CO_2 molecules by hydrogen bonding. It is essential to incorporate the molecular specifics of their CO_2-sorbent interactions in order to fabricate superior carbon-capture systems. Hence, the inclusion of a basic moiety into the polymers leads to a greater affinity to CO_2. Amidoximes are

[a]*Department of Physics, COMSATS Institute of Information Technology, Islamabad 44000, Pakistan*
[b]*Department of Chemistry, Quaid-i-Azam University, Islamabad-45320, Pakistan. E-mail: ilyassarwar@hotmail.com; Fax: +92-51-90642241; Tel: +92-51-90642132*
[c]*Department of Chemical Engineering, Qatar University, PO Box: 2713, Doha, Qatar. E-mail: mert.atilhan@qu.edu.qa; Fax: +974-4403-2491; Tel: +974-4403-4142*
[d]*Graduate School of EEWS, KAIST, 335 Gwahangno, Yuseong-gu, Daejeon, 305-701, Republic of Korea. E-mail: yavuz@kaist.ac.kr; Fax: +82-42-350-2248; Tel: +82-42-350-1718*

This journal is © The Royal Society of Chemistry 2013

Published on 15 July 2013. Downloaded by Pennsylvania State University on 18/09/2016 01:02:11.

an important class of organic compounds featuring a fused, basic amide and oxime functionality. These compounds are widely used in the pharmaceutical industry and as antitumor and antimalarial agents, polymers and chelating resins.[33–35] Polyamidoximes derived from acrylonitrile-divinylbenzene–vinylidene chloride copolymer beads with a porous structure have been reported.[36,37] These chelating resins were used as an ion-exchanger and as an adsorbent to uptake uranium from sea water.[38] The adsorption behavior of poly(acrylamidoxime) chelating resin for Cu(II), Cd(II), Hg(II), Zn(II), Pb(II), Cr(III), and U(VI) was investigated. This study shows that this resin had higher binding capacity to uranyl ions, fast kinetics, and very good selectivity from binary metal ion mixtures with Cu(II) and Pb(II).[39] Polyacrylonitrile fiber containing amidoxime groups with high adsorption capacity to Au^{3+} ions has been described.[40] Poly(amidoxime)–poly(hydroxamic acid) resins and fibers have also been investigated for the extraction of uranium from sea water.[41] Amidoximes are very similar in structure to monoethanolamine (MEA), which is a well known industrial standard for CO_2 capture, thus creating interest to explore their function as CO_2 adsorbents.

The aromatic polyamides, commonly referred as aramids, have been particularly useful as high-performance materials because of their very high thermal stability, stiffness, specific strength, and low density.[42–44] The inflexible features of such polymers made them as high-performance materials which is the main disadvantage in many applications. However, most aramids suffer poor processability due to limited solubility in common organic solvents and high glass transition (T_g) and softening (T_s) temperatures. Therefore, significant efforts have been made to increase the solubility and processability of aramids by structural modification. Soluble aramids may open applications in films, separation membranes, coatings, polymer blends, and composites.[45,46] For gas capture applications, aramids can prove useful with their remarkable strength in harsh conditions such as power plant exhaust fumes.

We recently showed[47] that amidoximes exhibit improved CO_2 capture capacities when compared with similar porous solids.[48–51] The challenge, however, was that the overall efficacy lacked promise for large scale applications, where high throughput processes with robust materials are necessary. In the present attempt, we successfully incorporated amidoxime pendant groups to aramid backbones and observed a significant increase in CO_2 capture capacity. The new durable solids are found to be viable candidates for power plant CO_2 scrubbing. To the best of our knowledge, aramids or porous polymers with amidoxime functional groups have never been reported.

2. Experimental

2.1. Materials

4,4′-Oxydianiline (ODA) (⩾98%), *p*-phenylenediamine (*p*-PDA) (⩾99%), potassium cyanide (98%) and ethanol (99%) were procured from Fluka. 5-Aminoisophthalic acid (94%), copper(I) cyanide (99.98%), sodium carbonate (99.99%), hydrochloric acid (37%), ammonium hydroxide (⩾99.99%), hydroxylamine solution (50 wt.% in H_2O) (99.9%), 1-methyl-2-pyrrolidinone (NMP) (⩾99.5%) and sodium nitrite (99.999%) were supplied by Aldrich and used as received.

2.2. Characterization

FTIR spectra of monomer and polymers were recorded at room temperature using an Excalibur Series FTIR spectrometer, model no. FTSW 300 MX, manufactured by BIO-RAD. NMR spectra were taken at room temperature using a BRUKER spectrometer operating at 300 MHz for ^{1}H and at 75 MHz for ^{13}C NMR in deuterated dimethyl sulfoxide (DMSO-d_6). Tetramethylsilane was used as an internal reference. Thermal stability of the polymers was determined by a Mettler Toledo TGA/SDTA 851^e thermogravimetric analyzer at a heating rate of 10 °C min^{-1} under N_2 atmosphere. Glass transition temperatures of the polymers were determined using a Mettler Toledo DSC 822^e differential scanning calorimeter in N_2 at a heating rate of 10 °C min^{-1}. X-ray diffraction measurements were performed on a Rigaku (D/Max-2500) HR-X-ray diffractometer using Ni-filtered Cu-Kα radiation at 40 kV and 300 mA. The surface morphology of powdered polymer samples was investigated by an FEI Nova 230 field emission scanning electron microscope (FESEM). Nitrogen adsorption–desorption isotherms were measured at 77 K using a Tristar 3020, Micromeritics (USA) porosimetry analyzer. For surface area determination, the Brunauer–Emmett–Teller (BET) method was employed using a nitrogen molecule surface area of 0.162 nm^2. The powdered aramid samples were degassed for surface area analysis at 100 °C for 6 h under vacuum. A Tristar 3000, Micromeritics (USA) CO_2 analyzer was used to determine CO_2 adsorption capacity at pressure of 1 bar.

2.3. High pressure CO_2 adsorption studies

Gravimetric carbon dioxide adsorption capacities of amidoxime porous polymer APP-1 and APP-2, were monitored at 318 K up to 225 bar using a high-pressure magnetic suspension balance (MSB) made by Rubotherm Präzisionsmesstechnik GmbH. The balance was maintained at 373 K up to 350 bars with two different operating positions as illustrated in Fig. 1. Firstly, the measuring cell was loaded with CO_2 at the sorption position. The MSB measured the change in weight of the sample upon adsorption of high pressure gas on it. The second position was used to determine the *in situ* density of the high-pressure gas needed to calculate the amount of adsorbed gas on the solid sample in the high-pressure cell. The change in weight of a sorbent sample is usually measured in the gravity field upon adsorption from a surrounding gas phase *via* a contactless force transmission method; which allows more stable operation at high pressures. The increase in weight of the sample within the cell is conveyed through magnetic suspension coupling from a closed and pressure-proof metal container to an external microbalance. The cell is provided with a platinum resistance thermometer, Jumo DMM 5017 Pt100, that records the cell temperature within ± 273 K accuracy. The pressure is measured with a Paroscientific® Digiquartz 745-3K with an accuracy of 0.01%.

 This journal is © The Royal Society of Chemistry 2013

Published on 15 July 2013. Downloaded by Pennsylvania State University on 18/09/2016 01:02:11.

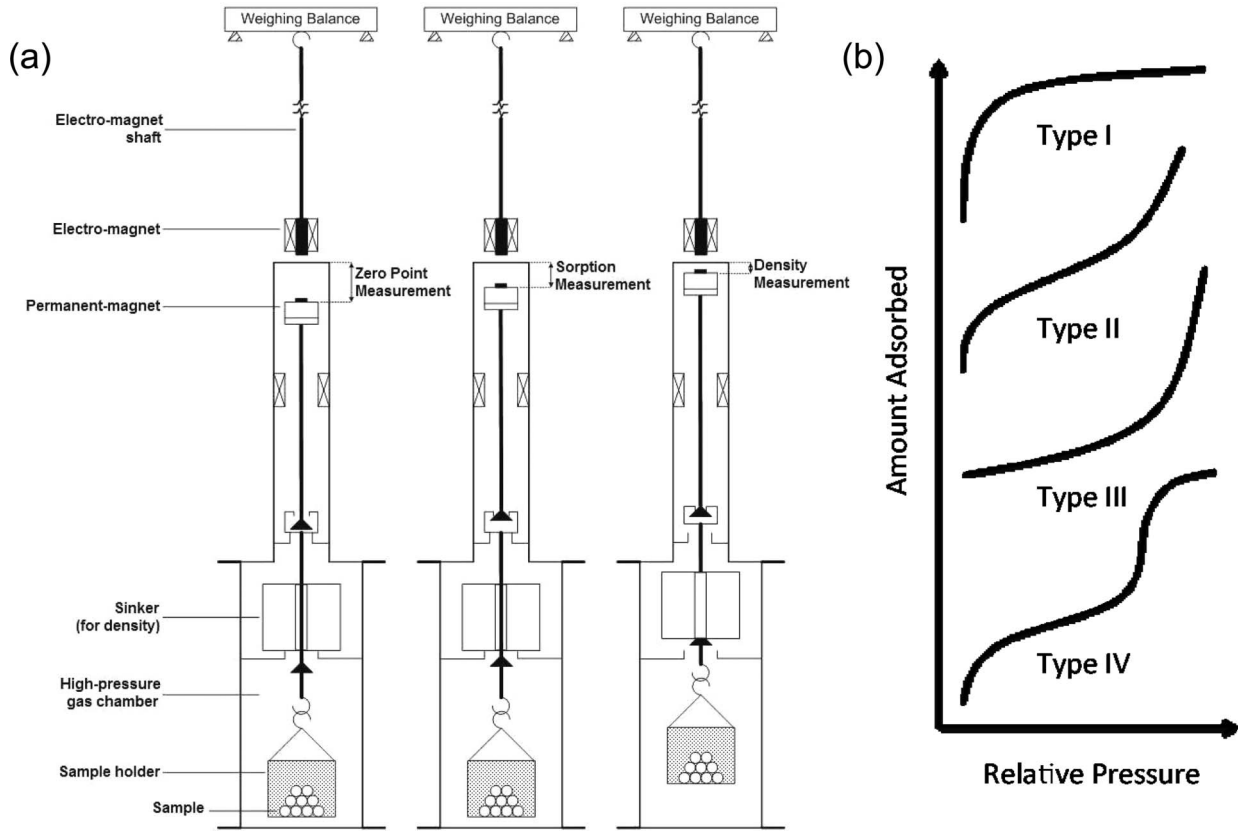

Fig. 1 (a) Schematics of the MSB and its operation positions used for sorption and density measurements. (b) Types of isotherms that are common to gas adsorption experiments.

Typical measurements were conducted by taking 0.25 g of sample in the holder and evacuating the system for 24 h at 333 K. CO_2 was then pressurized with the help of a Teldyne Isco 260D fully automated gas booster and added into the high-pressure cell, where CO_2 adsorption on the sample commenced. For each pressure point it took 45 min to reach equilibrium and once it was reached, 4 different set of measurements were recorded for a period of 10 min; each data point was taken at 30 s interval. The total span for each temperature and pressure point took around 50 min. At the end of each pressure point, the system automatically moved to the next pressure measurement point. The optimum pressure up to 225 bars was used in the present work and at the end of each isotherm, a hysteresis check was carried out at each isotherm by collecting desorption data as the system was depressurized. The adsorption data was evaluated and the amount of adsorbed CO_2 was calculated using the following relationship:

$$W + W_{\text{buoy,sample}} + W_{\text{buoy,sinker}} = m_{\text{ads}} + m_{\text{sample}} + m_{\text{sinker}} \quad (1)$$

where: W= signal read by the instrument; $W_{\text{buoy,sample}} = V_{\text{sample}} \times d_{\text{gas}}$ = buoyancy correction due to sample; V_{sample} = volume of the sample; d_{gas} = density of the gas; $W_{\text{buoy,sinker}} = V_{\text{sinker}} \times d_{\text{gas}}$ = buoyancy correction due to sinker; V_{sinker} = volume of the sinker; m_{ads} = adsorption amount; m_{sample} = mass of the sample; and m_{sinker} = mass of the sinker.

The density of gas was recorded *in situ* by the second measurement position (Fig. 1) and verified with REFPROP 9.0[52] for accurate measurements. The mass of empty sinker was taken at numerous pressures of helium to find out the buoyancy due to the sinker. The volume of sinker was computed from the slope of a weight *vs.* density plot. A blank reading under vacuum was recorded to measure the mass of the sinker. The buoyancy correction due to the sample was achieved by calculating the volume of the sample obtained by the slope of a weight *vs.* density plot similar to the helium measurement of the sinker with the sample. The mass of the sample was recorded under vacuum and activated charcoal norit® RB3 was employed for calibration. The CO_2 adsorption–desorption behavior of both aramids was monitored by exposing the sample to increasing and decreasing pressure increments of CO_2 at a particular temperature. The sample and gas were permitted to reach equilibrium at each pressure point. The corresponding mass change was then corrected for buoyancy to achieve the adsorption amount (mmoles of CO_2 per g of adsorbent).

Regardless of the measurement method, gas adsorption follows certain pre-defined isotherms based on the pore size and distribution (Fig. 1b). The types I–IV are most common, although more exist. In a typical Type I isotherm, a Langmuir

Published on 15 July 2013. Downloaded by Pennsylvania State University on 18/09/2016 01:02:11.

coverage is observed where gas molecules can only find enough space to form a simple monolayer. This is typical for predominantly microporous solids such as activated carbons and zeolites, with negligible inter-particle voids. Accessibility of the micropores governs the uptake. Type II is found mostly in macroporous or non-porous structures where monolayer coverage (the first saturation) is followed by a multi-layer adsorption. The isotherm does not reach equilibrium at the end, pointing to an unrestricted exchange between mono and multi layer stages. Type III is not too common but nonetheless exists. It should be considered as Type II without, or with negligible, initial saturation. Type IV is characteristic of mesoporous solids and should be considered as the combination of the capillary filling effects of mesopores with that of Type II (and possible Type I). The final saturation represents the lesser contribution of macro or inter-particle pores.

2.4. Synthesis of 5-cyanoisophthalic acid (1)

5-Aminoisophthalic acid (0.02 mol, 3.62 g), conc. HCl (5 mL) and distilled H_2O (5 mL) were placed in a 250 mL round bottom flask provided with a magnetic stirrer. The reaction mixture was agitated for 25 min and cooled to 0 °C in an ice-bath. After complete mixing, $NaNO_2$ solution (prepared by dissolving 0.023 mol, 1.58 g of $NaNO_2$ in 4 mL of H_2O) was added drop-wise into the flask resulting in yellow colored diazonium chloride. The diazonium chloride was poured into hot cyanide solution (prepared by dissolving 0.069 mol, 4.49 g of KCN and 0.023 mol, 2.06 g of CuCN in 13 mL of water with Na_2CO_3 (2 g) at 60 °C for 10 min). Then the mixture was cooled to room temperature, followed by the addition of conc. HCl until no more precipitates were formed. The yellow precipitates were filtered off, washed with water and treated with NH_4OH (14 mL). Further filtration and acidification of the filtrate with conc. HCl produced the light orange precipitate of 5-cyanoisophthalic acid (Scheme 1), which was purified by recrystallization in water. Finally, the product was dried under reduced pressure at 80 °C for 24 h. Yield (85%); FTIR (KBr) 2500–3500 cm^{-1} (acid O–H stretch), 3060 cm^{-1} (aromatic C–H stretch), 1715 cm^{-1} (C=O stretch), 2246 cm^{-1} (C≡N stretch), 1646, 1438 cm^{-1} (aromatic C=C stretch). ^{1}H NMR: δ_H (300 MHz, DMSO-d_6) 9.27(1H, s), 8.71 (2H, s); 13.65 (2H, s). ^{13}C NMR: δ_C (75 MHz, DMSO-d_6) 112.8, 115.8, 131.1, 135.2, 139.2, 169.5.

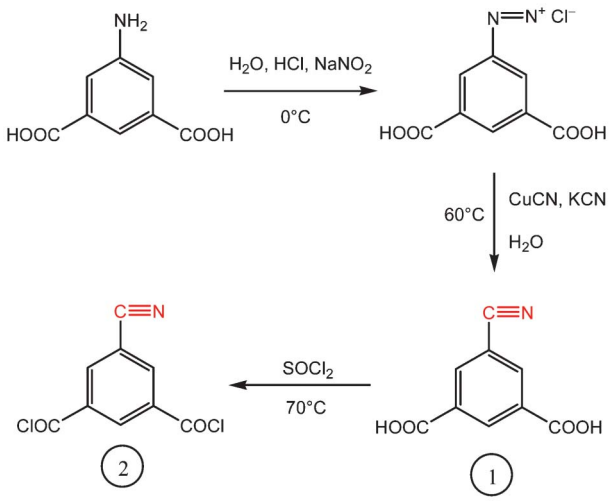

Scheme 1 Synthesis of 5-cyanoisophthalic acid and 5-cyanoisophthaloyl chloride.

2.5. Synthesis of 5-cyanoisophthaloyl chloride (2)

5-Cyanoisophthalic acid (0.11 mol, 22 g) and thionyl chloride (13 mL) were refluxed for 1 h at 70 °C in a 250 mL round bottom flask. Excess of thionyl chloride was stripped off by distillation to obtain acid chloride with good yield (Scheme 1). Yield (80%); FTIR (KBr) 3088 cm^{-1} (aromatic C–H stretch), 1752 cm^{-1} (C=O stretch), 2244 cm^{-1} (C≡N stretch), 1644, 1435 cm^{-1} (aromatic C=C stretch), 692 cm^{-1} (C–Cl stretch). ^{1}H NMR: δ_H (300 MHz, DMSO-d_6) 9.12(1H, s), 8.66 (2H, s); ^{13}C NMR: δ_C (75 MHz, DMSO-d_6) 113.2, 115.9, 134.1, 137.3, 141.9, 167.5.

2.6. Synthesis of aramid bearing nitrile groups derived from ODA (3)

ODA (0.05 mol, 10.0 g) and 100 mL of NMP were charged into a 250 mL round bottom flask, equipped with a dropping funnel, gas inlet tube and a magnetic stirrer. After complete mixing of the diamine solution, 5-cyanoisophthaloyl chloride (0.05 mol, 11.4 g) dissolved in NMP (100 mL) was added dropwise to the above solution at 0 °C with constant stirring for 10 min and then at 25 °C for 24 h in a N_2 atmosphere. The reaction mixture was poured into water with continuous stirring and precipitates of the resulting polyamide having nitrile pendant groups were filtered off and thoroughly washed with hot water and dried under vacuum at 80 °C for 24 h (Scheme 2). Yield (74%); FTIR (KBr), 3310 cm^{-1} (N–H stretch), 3069 cm^{-1} (aromatic C–H stretch), 1603, 1494 cm^{-1} (aromatic C=C stretch), 1650 cm^{-1} (C=O stretch), 1214 cm^{1} (C–O–C stretch), 2234 cm^{-1} (C≡N stretch). ^{1}H NMR: δ_H (300 MHz, DMSO-d_6) 7.86 (1H, s), 6.85 (4H, d), 7.63 (4H, d) 8.42 (2H, s), 8.54 (1H, s); ^{13}C NMR: δ_C (75 MHz, DMSO-d_6) 112.6, 115.9, 119.5, 121.0, 129.6, 134.1, 135.2, 138.4 150.6, 165.1.

2.7. Synthesis of APP-1 (4)

The dried polyamide (**3**) containing nitrile groups (1 g) was dispersed in water (98.8 g) followed by the addition of hydroxylamine solution (50 wt.% in H_2O) (0.2044 g) with uninterrupted agitation and refluxing at 100 °C for 4 h. The contents of the flask were centrifuged to isolate the precipitates of amidoximated polyamide which were then washed with distilled water and dried under vacuum at 50 °C for 24 h (Scheme 2). Yield (68%); FTIR (KBr), 3309 cm^{-1} (N–H stretch), 3075 cm^{-1} (aromatic C–H stretch), 1606, 1498 cm^{-1} (aromatic C=C stretch), 1654 cm^{-1} (C=N and C=O stretch), 3198 cm^{-1} (O–H stretch), 1407 cm^{-1} (C–N stretch), 1232 cm^{-1} (C–O–C stretch), 955 cm^{-1} (N–O stretch). ^{1}H NMR: δ_H (300 MHz, DMSO-d_6) 7.83 (1H, s), 8.62 (1H, s), 5.97 (2H, s), 6.87 (4H, d), 8.50 (1H, s), 8.41 (2H, s), 7.62 (4H, d); ^{13}C NMR: δ_C (75 MHz, DMSO-d_6) 117.3, 121.1, 122.6, 134.3, 134.9, 135.7, 140.5, 150.5, 164.9, 165.2.

 This journal is © The Royal Society of Chemistry 2013

Published on 15 July 2013. Downloaded by Pennsylvania State University on 18/09/2016 01:02:11.

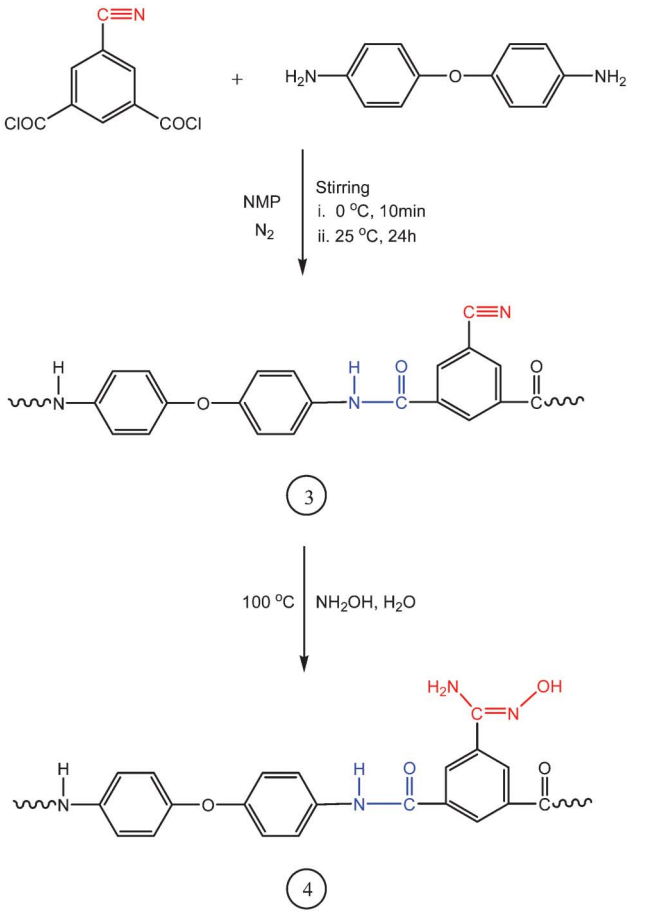

Scheme 2 Scheme for the synthesis of aramid bearing nitrile and amidoxime pendant groups derived from ODA.

2.8. Synthesis of aramid bearing nitrile groups derived from *p*-PDA (5)

The polymerization of *p*-PDA (0.05 mol, 5.4 g) and 5-cyanoisophthaloyl chloride (**2**) (0.05 mol, 11.4 g) was carried out in NMP. For this purpose, *p*-PDA was dissolved in NMP (100 mL), followed by the drop wise addition of 5-cyanoisophthaloyl chloride (**2**) dissolved in 100 mL NMP at 0 °C with continuous stirring for 10 min and then at 25 °C for 24 h in an inert atmosphere. The polymer was precipitated in water and filtered off (Scheme 3), thoroughly washed and dried. Yield (83%); FTIR (KBr), 3308 cm^{-1} (N–H stretch), 3101 cm^{-1} (aromatic C–H stretch), 1613, 1512 cm^{-1} (aromatic C=C stretch), 1651 cm^{-1} (C=O stretch), 2237 cm^{-1} (C≡N stretch). ^{1}H NMR: δ_H (300 MHz, DMSO-d_6) 8.61 (1H, s), 9.64 (1H, s) 8.80 (2H, s) 7.82 (4H, s); ^{13}C NMR: δ_C (75 MHz, DMSO-d_6) 112.6, 118.2, 121.6, 131.4, 132.8, 135.1, 138.2, 164.5.

2.9. Synthesis of APP-2 (6)

Similarly, an aramid bearing amidoxime groups (APP-2) was prepared by dispersing polyamide (**5**) in water and refluxing with hydroxylamine to convert the nitrile group into an amidoxime functionality. The precipitates of amidoximated polyamide were isolated, washed with distilled water and dried under vacuum for 24 h (Scheme 3). Yield (75%); FTIR (KBr), 3307 cm^{-1} (N–H stretch), 3105 cm^{-1} (aromatic C–H stretch), 1617, 1514 cm^{-1} (aromatic C=C stretch), 1655 cm^{-1} (C=N and C=O stretch), 3200 cm^{-1} (O–H stretch), 1402 cm^{-1} (C–N stretch), 938 cm^{-1} (N–O stretch). ^{1}H NMR: δ_H (300 MHz, DMSO-d_6) 8.42(1H, s), 9.89 (1H, s), 5.86 (2H, s), 8.62(1H, s), 8.52 (2H, s) 7.81 (4H, s); ^{13}C NMR: δ_C (75 MHz, DMSO-d_6) 124.3, 129.6, 132.8, 134.8, 135.3, 138.6, 164.6, 166.0.

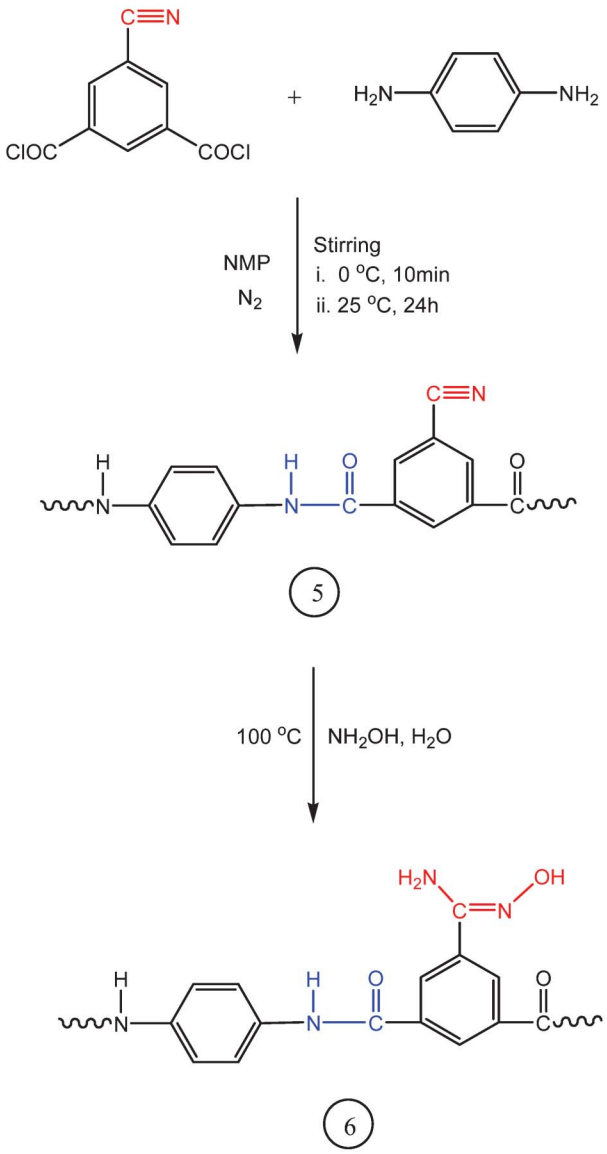

Scheme 3 Scheme for the synthesis of aramid bearing nitrile and amidoxime pendant groups derived from *p*-PDA.

3. Results and discussion

3.1. Monomer and polymer synthesis

Aramids are polymers with exceptional stability and rigidity, finding good use in applications that require highly resistant media (*e.g.* Kevlar®). In membrane or sorbent developments,

Published on 15 July 2013. Downloaded by Pennsylvania State University on 18/09/2016 01:02:11.

however, soft texture and processability emerge as more crucial properties. Numerous attempts have been made to modify the structure of aramids to make them more soluble and processable.[53] Among them, the introduction of different flexible linkages and kinks (–O–, $–SO_2–$, $–CH_2–$, $–C(CF_3)_2–$ *etc.*) along the back bone led to significant improvement in the solubility of aramids in many polar aprotic solvents like DMF, DMAc, DMSO, NMP *etc.*[54] Another interesting approach to modify the structure of aramids is the incorporation of bulky substituents as pendant groups in the main chain. So, by carefully selecting the pendant group, solubility can easily be promoted without affecting other properties. In this regard, amidoxime groups may deliver enhanced processability, along with their use for CO_2-philic behavior.

The synthesis involved the conversion of the amine group of 5-aminoisophthalic acid (**1**) into a nitrile group, which upon reaction with thionyl chloride produced 5-cyanoisophthaloyl chloride (**2**) (Scheme 1). Aramids were then synthesized by condensing 5-cyanoisophthaloyl chloride with ODA or *p*-PDA at low temperature and amidoxime groups were introduced by converting the nitrile groups using hydroxylamine solution (Schemes 2 & 3). The structure elucidation of both monomer and aramids were carried out by FTIR, ^{1}H and ^{13}C NMR spectroscopy. The resulting aramids APP-1 and APP-2 were then further characterized for organosolubility, thermal stability, glass transition temperatures, X-ray diffraction, FESEM, BET analysis and CO_2 adsorption measurements.

3.2. Organosolubility

Both the polyamides bearing amidoxime groups were soluble in polar aprotic solvents such as DMSO, DMF, and NMP while being insoluble in others such as THF, methanol and chloroform. Table 1 shows qualitative solubility data of both the aramids in some common solvents (DMF, NMP, DMSO, THF, CH_3OH, $CHCl_3$ and *m*-cresol). Polyamide APP-1 derived from the condensation of ODA and 5-cyanoisophthaloyl chloride dissolves rapidly at room temperature because of the flexible ether linkages in the backbone. Alternatively, the lower solubility of polyamide APP-2 at room temperature is attributed to the rigid aromatic unit (*p*-phenylene) in the polyamide chains.

3.3. Thermal analyses

The thermal stability of CO_2 adsorbents is crucial for practical applications; therefore, thermal behavior of the aramids was determined through thermogravimetric analysis (TGA) and differential scanning calorimetry (DSC) in a N_2 atmosphere at a heating rate of 10 °C min^{-1}. The thermograms revealed that both polymers were thermally stable (Fig. 2). However, the thermal stability of APP-2 was higher than APP-1, which has weak ether linkages in the backbone thereby exhibiting lower thermal stability relative to APP-2. The glass-transition temperature (T_g) of APP-1 was at 97 °C and APP-2 at 242 °C (Fig. 3). Generally, the inclusion of rigid units along a polymer backbone restricts the segmental mobility responsible for increased T_g values.[55] On the contrary, flexible linkages reduce the rigidity and T_gs of the polymers. Therefore, depending on the structure of the diamine component, the glass-transition temperatures of the aramids increased with higher rigidity and symmetry of the polymer backbone. Polyamide APP-2 containing *para* units displayed higher T_g values because these units suppressed the segmental mobility in the polymer chains. Predictably, polyamide APP-1 having flexible ether linkages showed relatively lower T_g values on account of enhanced segmental/molecular mobility.

Table 1 Solubility behavior of aramids containing amidoxime pendant groups[a]

Polymer	DMSO	DMF	NMP	THF	*m*-cresol	Methanol	Chloroform
APP-1	++	++	++	–	+–	–	–
APP-2	++	++	++	–	–	–	–

[a] Solubility: ++ Soluble at room temperature. +– Partially soluble at room temperature. – Insoluble.

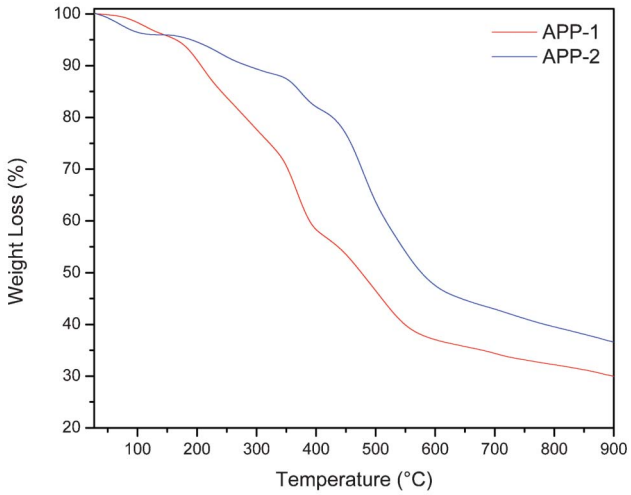

Fig. 2 TGA curves of aramids APP-1 and APP-2.

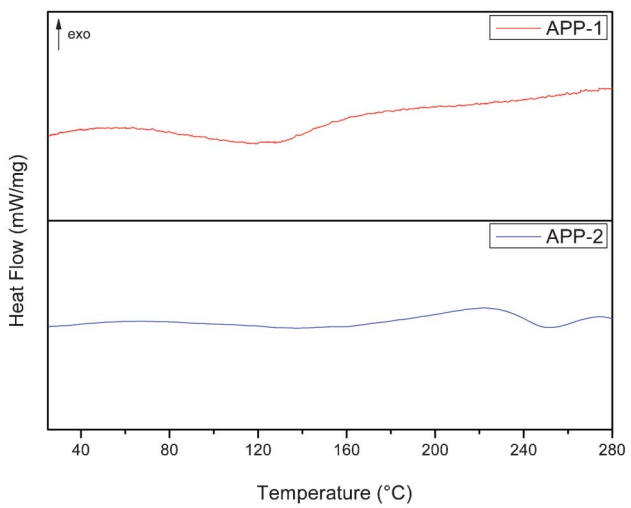

Fig. 3 DSC thermograms of aramids APP-1 and APP-2.

 This journal is © The Royal Society of Chemistry 2013

Published on 15 July 2013. Downloaded by Pennsylvania State University on 18/09/2016 01:02:11.

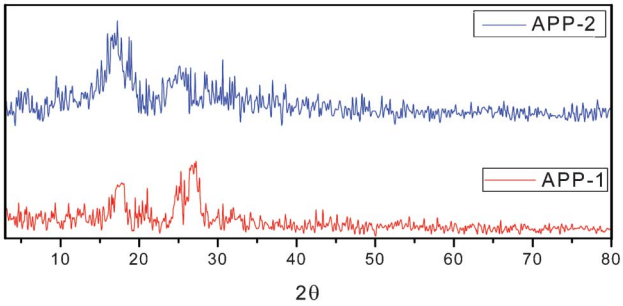

Fig. 4 PXRD patterns of aramids APP-1 and APP-2.

3.4. X-ray diffraction

XRD patterns of the polyamides are illustrated in Fig. 4. Polyamide APP-1 with ether groups showed a relative decrease in crystalline behavior owing to the presence of C–O–C linkages in the polymer backbone that gives rise to less close chain packing or aggregation giving a weak diffraction pattern. Conversely, polyamide APP-2 displayed a crystalline peak at around 17° due to the existence of rigid units in the macromolecular backbone leading to an efficient close packing of the polymer chains. Generally, solubility increases with decreasing crystallinity as evident in the case of polyamide APP-1 that shows increased solubility in polar solvents at room temperature compared with polyamide APP-2. Correspondingly, XRD results were authenticated by thermal analysis wherein polyamide APP-2 demonstrated higher T_g values.

3.5. Structural characterization

The porous nature of the polyamides was evaluated by N_2 uptake measured at 77 K (Fig. 5). Structural parameters calculated from N_2 adsorption isotherms are presented in Table 2. The BET surface area was calculated by applying the Brunauer–Emmett–Teller (BET) model. Polyamides APP-1 and APP-2 encompassed apparent surface areas of 49.5 $m^2\ g^{-1}$ and 0.67 $m^2\ g^{-1}$, respectively. The total pore volumes calculated for polyamides APP-1 and APP-2 were found to be 0.24 and 0.001 $cm^3\ g^{-1}$, while the average pore sizes were 16.9 and 9.9 nm respectively. The N_2 sorption isotherms of polyamides APP-1 and APP-2 exhibited "Type III" and "Type II" behaviors.

3.6. Field emission scanning electron microscopy

The surface morphology of the aramid samples (**4**) and (**6**) was investigated by field emission scanning electron microscopy. The micrographs of the polyamides are shown in Fig. 6. The FESEM image of polyamide APP-1 revealed significant macroporosity in the sample whereas polyamide APP-2 has an almost non-porous structure which may be explained on the basis of molecular configuration. The micrograph (Fig. 6a) clearly indicates that APP-1 has more free volume and shows a less compact structure, therefore it exhibits a more porous nature. Meanwhile the FESEM image of APP-2 (Fig. 6b) displays a highly compact structure and less free volume thus signifying a nonporous morphology. The gas adsorption displayed by polyamide APP-1 therefore confirmed the porous nature of the material. On the other hand, polyamide APP-2 demonstrated a lower N_2 uptake owing to the nonporous nature of the sample.

3.7. Low pressure CO_2 adsorption measurements

CO_2 uptake by fully organic polymers is emerging as an alternative for industrial CO_2 scrubbing processes.[56] To authenticate the potential of modified aramids as CO_2 sorbents, two different types of aramids bearing amidoxime pendant groups were prepared having flexible and rigid groups in the polymer backbone for comparative study using a facile synthetic approach of treating the nitrile pendant group with hydroxylamine. CO_2 uptake of both aramids, APP-1 and APP-2, was carried out at two different temperatures, 273 K and 298 K, at a pressure of 1 bar. The CO_2 adsorption capacity of APP-1 was found to be 0.32 mmol g^{-1} at 273 K, which decreased to 0.19 mmol g^{-1} with an increase in temperature to 298 K. Likewise, the adsorption isotherms of APP-2 at 273 K indicated 0.07 mmol g^{-1} uptake of CO_2 which also reduced to 0.05 mmol g^{-1} at 298 K (Fig. 7 and Table 3). The adsorption capacities decreased drastically when the temperature was increased from 273 K to 298 K, inferring that the CO_2 adsorption capacity is very much dependant on temperature. These CO_2 adsorption capacities of both aramids are in good agreement with the

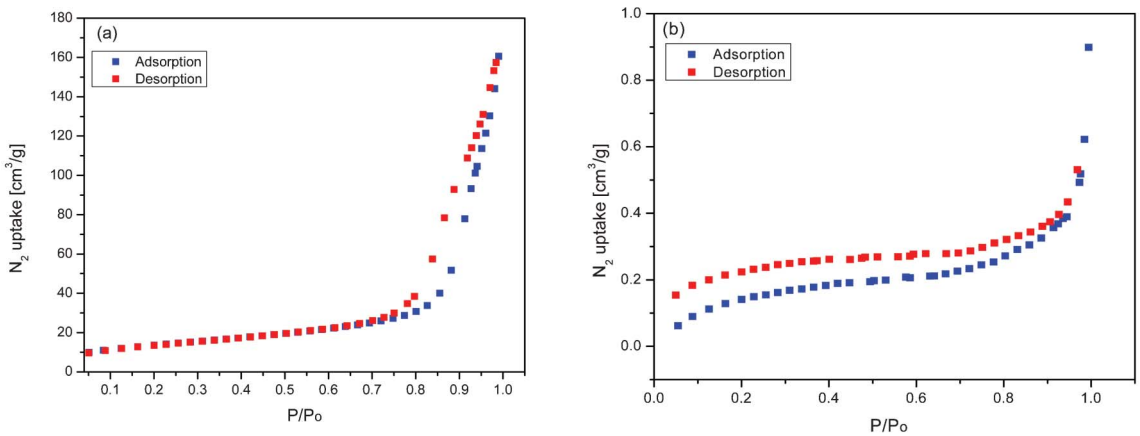

Fig. 5 N_2 isotherms for (a) APP-1 (b) APP-2 measured at 77 K.

Published on 15 July 2013. Downloaded by Pennsylvania State University on 18/09/2016 01:02:11.

Table 2 Textural parameters calculated from N_2 adsorption isotherms at 77 K

Parameter	APP-1	APP-2
BET surface area ($m^2\ g^{-1}$)	49.5	0.67
Langmuir surface area ($m^2\ g^{-1}$)	68.0	1.120
Average pore size (nm)	16.9	9.90
Pore volume ($cm^3\ g^{-1}$)	0.24	0.001

fact that the extent of physical adsorption decreases with an increase in temperature because of the exothermic nature of the binding.[57] The adsorption behavior for both the aramids showed a substantial chemical interaction with the gas molecules, which would be attributed to the affinity of the acidic CO_2 molecule towards the basic NH_2 group of the amidoxime pendant group. The reasonable CO_2 adsorption capacity of aramid APP-1 over APP-2 was also due to the difference in porosity of the material where the presence of flexible ether linkages in the polymer backbone hinders the close packing of polymer chains resulting in the availability of amidoxime functional groups on the surface of the aramid. Alternatively, APP-2 displayed less affinity towards CO_2 adsorption which was ascribed to the rigid aromatic groups in the aramid backbone leading to close chain packing responsible for the decrease in porosity. The adsorption isotherms of both aramids exhibit "Type I" behavior at 273 K and 298 K, depicting a monolayer adsorption.

An adsorption–desorption hysteresis appeared with both the polymers studied, particularly at low pressure. Ideally, desorption isotherms should not deviate from the sorption isotherms. However, as is evident from Fig. 7, the desorption isotherms generally lie above the excess sorption isotherms, *i.e.* a significant hysteresis effect is associated with the sorption–desorption process. This hysteresis effect indicated that the sorbent–sorbate system is in a metastable state and as the pressure decreases, the gas is not readily released to the extent corresponding to the thermodynamic equilibrium value. APP-1 showed the smallest deviations between adsorption and desorption curves (little hysteresis), which indicated that CO_2 can be almost fully recovered during desorption while the adsorption–desorption isotherms of APP-2 exhibited a strong hysteresis mainly in the lower pressure range. The empirical classification of a hysteresis loop was given by IUPAC in which the shape of the loop is correlated with the structure of the adsorbent.[58] APP-1 and APP-2 both produced an H4 type of hysteresis loop. H4 type loops are usually observed with complex materials containing both micropores and mesopores.[59] An H4 hysteresis contains a characteristic step-down in the desorption branch associated with the hysteresis loop closure. The hysteretic adsorption is not reversible in the sense that the ensuing adsorption isotherm does not retrace the previous desorption isotherm.

3.8. High pressure CO_2 adsorption measurements

CO_2 adsorption isotherms (Fig. 8) showed the augmentation in the adsorption capacity for both the polyamides studied at a high pressure of 225 bar at 318 K. To the best of our knowledge, these pressures are the highest ever studied in the literature. Of course, under these conditions, CO_2 is no longer a gas and the adsorption dynamics differ substantially; however, our goal is to cover as many parameters as possible to alleviate the challenges in developing a proper CO_2 sorbent that is immune to extreme conditions. In particular, the geological capture and pipeline (or container ships) transport processes require understanding how CO_2 behaves with or without porous structures at high pressures and temperatures.

The CO_2 uptakes of APP-1 and APP-2 were found to be 24.69 mmol g^{-1} and 11.67 mmol g^{-1} respectively at 225 bar and 318 K. The results revealed the escalating adsorption for both the polyamides at high pressure but the remarkable improvement in APP-1 adsorption above 70 bar is particularly noticeable. The adsorption isotherms of APP-1 and APP-2 exhibited "Type IV" behavior, in which multilayer adsorption was observed after the completion of the first layer. The adsorption isotherms of both polyamides maintained a clear distinction between the first layer (0–70 bar region) and multilayer (70–225 bar region) adsorptions depicting that the adsorbate–adsorbent interactions present in these polymers are the

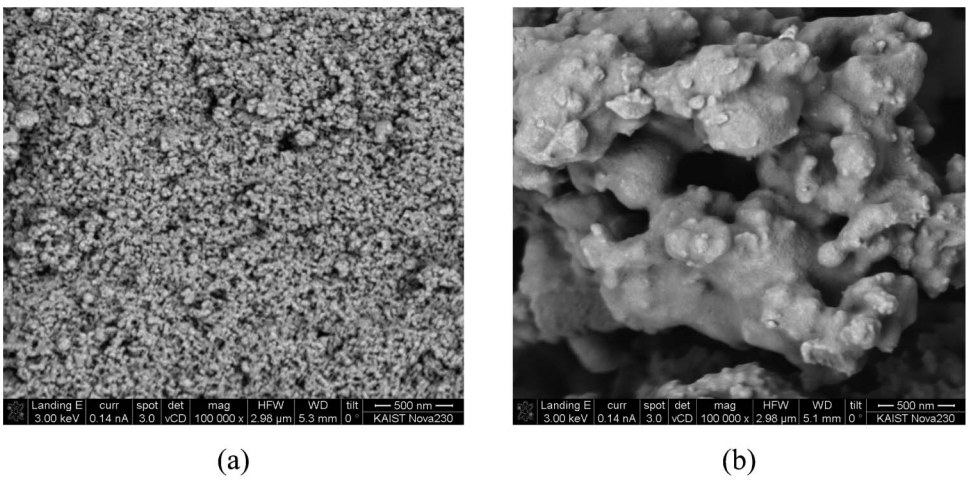

Fig. 6 FESEM micrographs of (a) APP-1 (b) APP-2.

 This journal is © The Royal Society of Chemistry 2013

Published on 15 July 2013. Downloaded by Pennsylvania State University on 18/09/2016 01:02:11.

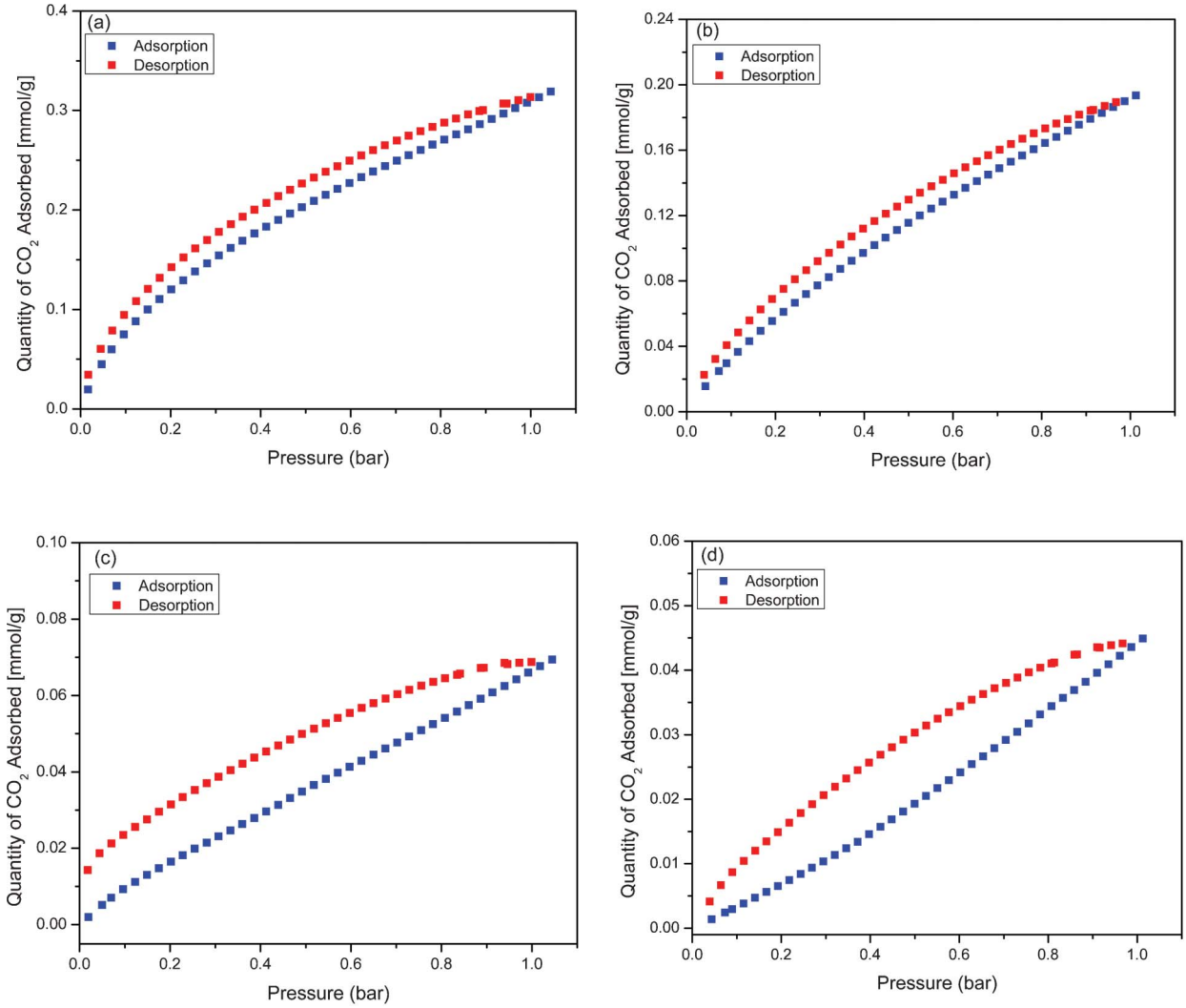

Fig. 7 CO_2 gas sorption isotherms at pressure of 1 bar (a) APP-1 at 273 K (b) APP-1 at 298 K and (c) APP-2 at 273 K (d) APP-2 at 298 K.

strongest. No hysteresis loop was observed for both the polymers at high pressure in contrast to low pressure because, at low pressure, chemisorption is the primary reason for the gas to interact, whereas at high pressure the amount of chemisorbed species decreased.

4. Conclusions

Exploitation of polyamides bearing amidoxime functionality as CO_2 scavengers showed that these macromolecules can serve as promising candidates for CO_2 capture and storage. Building on our earlier work[47] we now show that robust chains of aramids can host CO_2-active amidoxime units for enhanced CO_2 capture. The porous amidoxime polymers reported here are the first examples of this highly promising family of porous solids. In particular, we explored two types of aramids bearing amidoxime groups. CO_2 adsorption up to 0.32 mmol g^{-1} at 273 K and 1 bar was found for polyamide APP-1, which is considerable since aramids are usually non-porous hard supports and not expected to be CO_2-philic. The solubility of

Table 3 CO_2 Adsorption capacity (mmol g^{-1}) of aramids at 1 and 225 bar

Aramid	CO_2 Adsorbed (mmol g^{-1}) at 1 bar		CO_2 Adsorbed (mmol g^{-1}) at 225 bar
	T = 273 K	T = 298 K	T = 318 K
APP-1	0.32	0.19	24.69
APP-2	0.07	0.05	11.67

Published on 15 July 2013. Downloaded by Pennsylvania State University on 18/09/2016 01:02:11.

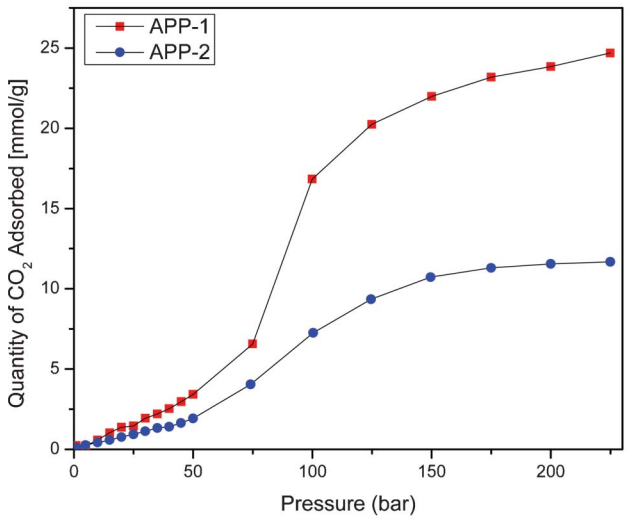

Fig. 8 CO_2 gas sorption isotherms of APP-1 and APP-2 at 225 bar and 318 K.

these new aramids also paves the way for membrane applications. By increasing the pressure up to 225 bar, the adsorption value increased to 24.69 mmol g^{-1} for APP-1 and 11.67 mmol g^{-1} for APP-2. This superior adsorption of polyamide APP-1 was attributed to its more porous nature when compared with APP-2.

Acknowledgements

This work was made possible by NPRP grants # 08-670-1-124 and #5-499-1-088 from the Qatar National Research Fund (a member of Qatar Foundation). The statements made herein are solely the responsibility of the authors. We also acknowledge the financial support by grants from the Korea CCS R&D Center, IWT (NRF-2012-C1AAA001-M1A2A2026588) funded by the Ministry of Education, Science and Technology of Korean government, the Basic Science Research Program through the National Research Foundation of Korea (NRF) funded by the Ministry of Science, ICT & Future Planning (2013R1A1A1012998), and the KAIST EEWS Initiative.

References

1 J. J. McCarthy, O. F. Canziani, N. A. Leary, D. J. Dokken and K. S. White, *Climate Change 2001: Impacts, Adaptation, and Vulnerability*, Cambridge University Press, Cambridge, 2001.
2 R. A. Kerr, *Science*, 2007, **316**, 188–190.
3 S. Lee, T. P. Filburn, M. Gray, J. W. Park and H. J. Song, *Ind. Eng. Chem. Res.*, 2008, **47**, 7419–7423.
4 J. C. Abanades, E. S. Rubin and E. J. Anthony, *Ind. Eng. Chem. Res.*, 2004, **43**, 3462–3466.
5 J. D. Figueroa, T. Fout, S. Plasynski, H. McIlvried and R. D. Srivastava, *Int. J. Greenhouse Gas Control*, 2008, **2**, 9–20.
6 M. T. Ho, G. W. Allinson and D. E. Wiley, *Ind. Eng. Chem. Res.*, 2008, **47**, 4883–4890.
7 G. P. Knowles, J. V. Graham, S. W. Delaney and A. L. Chaffee, *Fuel Process. Technol.*, 2005, **86**, 1435–1448.
8 M. L. Gray, Y. Soong, K. J. Champagne, J. Baltrus, R. W. Stevens Jr, P. Toochinda and S. S. C. Chuang, *Sep. Purif. Technol.*, 2004, **35**, 31–36.
9 X. Xu, C. Song, J. M. Andresen, B. G. Miller and A. W. Scaroni, *Microporous Mesoporous Mater.*, 2003, **62**, 29–45.
10 T. Filburn, J. J. Helble and R. A. Weiss, *Ind. Eng. Chem. Res.*, 2005, **44**, 1542–1546.
11 M. Radosz, X. Hu, K. Krutkramelis and Y. Shen, *Ind. Eng. Chem. Res.*, 2008, **47**, 3783–3794.
12 M. M. Maroto-Valer, Z. Tang and Y. Zhang, *Fuel Process. Technol.*, 2005, **86**, 1487–1502.
13 M. G. Plaza, C. Pevida, A. Arenillas, F. Rubiera and J. J. Pis, *Fuel*, 2007, **86**, 2204–2212.
14 C. Lu, H. Bai, B. Wu, F. Su and J. F. Hwang, *Energy Fuels*, 2008, **22**, 3050–3056.
15 C. Pevida, M. G. Plaza, B. Arias, J. Fermoso, F. Rubiera and J. J. Pis, *Appl. Surf. Sci.*, 2008, **254**, 7165–7172.
16 M. G. Plaza, C. Pevida, B. Arias, M. D. Casal, C. F. Martin, J. Fermoso, F. Rubiera and J. J. Pis, *J. Environ. Eng.*, 2009, **135**, 426–432.
17 C. Pevida, T. C. Drage and C. E. Snape, *Carbon*, 2008, **46**, 1464–1474.
18 T. C. Drage, J. M. Blackman, C. Pevida and C. E. Snape, *Energy Fuels*, 2009, **23**, 2790–2796.
19 H. Hayashi, J. Taniuchi, N. Furuyashiki and S. Sugiyama, *Ind. Eng. Chem. Res.*, 1998, **37**, 185–191.
20 N. Shigemoto, T. Yanagihara, S. Sugiyama and H. Hayashi, *Energy Fuels*, 2006, **20**, 721–726.
21 C. T. Yavuz, B. D. Shinall, A. V. Iretskii, M. G. White, T. Golden, M. Atilhan, P. C. Ford and G. D. Stucky, *Chem. Mater.*, 2009, **21**, 3473–3475.
22 J. Merel, M. Clausse and F. Meunier, *Ind. Eng. Chem. Res.*, 2008, **47**, 209–215.
23 D. Ko, R. Siriwardane and L. T. Biegler, *Ind. Eng. Chem. Res.*, 2003, **42**, 339–348.
24 S. Cavenati, C. A. Grande and A. E. Rodrigues, *J. Chem. Eng. Data*, 2004, **49**, 1095–1101.
25 A. D. Ebner and J. A. Ritter, *Sep. Sci. Technol.*, 2009, **44**, 1273–1421.
26 J. A. Ritter and A. D. Ebner, *Sep. Sci. Technol.*, 2007, **42**, 1123–1193.
27 J. Yang, C. H. Lee and J. W. Chang, *Ind. Eng. Chem. Res.*, 1997, **36**, 2789–2798.
28 C. Song, *Catal. Today*, 2006, **115**, 2–32.
29 X. Xiaoding and J. A. Moulijn, *Energy Fuels*, 1996, **10**, 305–325.
30 J. F. Jenck, F. Agterberg and M. J. Droescher, *Green Chem.*, 2004, **6**, 544–556.
31 N. MacDowell, N. Florin, A. Buchard, J. Hallett, A. Galindo, G. Jackson, C. S. Adjiman, C. K. Williams, N. Shah and P. Fennell, *Energy Environ. Sci.*, 2010, **3**, 1645–1669.
32 G. T. Rochelle, *Science*, 2009, **325**, 1652–1654.
33 K. P. Flora, B. Vantriet and G. L. Wampler, *Cancer Res.*, 1978, **38**, 1291–1295.
34 J. B. Hynes and L. G. Hack, *J. Med. Chem.*, 1972, **15**, 1194–1196.
35 B. L. Rivas, H. A. Maturana and S. Villegas, *J. Appl. Polym. Sci.*, 2000, **77**, 1994–1999.

 This journal is © The Royal Society of Chemistry 2013

Published on 15 July 2013. Downloaded by Pennsylvania State University on 18/09/2016 01:02:11.

36 N. Kabay and H. Egawa, *Sep. Sci. Technol.*, 1993, **28**, 1985–1993.
37 N. Kabay, T. Hayashi, A. Jyo and H. Egawa, *J. Appl. Polym. Sci.*, 1994, **54**, 333–338.
38 H. Egawa, N. Kabay, A. Jyo, M. Hirono and T. Shuto, *Ind. Eng. Chem. Res.*, 1994, **33**, 657–661.
39 B. L. Rivas, H. N. A. Maturana and S. Villegas, *J. Appl. Polym. Sci.*, 2000, **77**, 1994–1999.
40 W. Lin, Y. Lu and H. Zeng, *J. Appl. Polym. Sci.*, 1993, **47**, 45–52.
41 F. Vernon and T. Shah, *React. Polym., Ion Exch., Sorbents*, 1983, **1**, 301–308.
42 J. F. Wolfe, Polyamides, Aromatic, in *Encyclopedia of Polymer Science and Engineering*, ed. H. F. Mark, N. M. Bikales, C. G. Overberger and G. Menges, Wiley, New York, 1987, p. 635.
43 P. E. Cassidy, *Thermally Stable Polymers*, Dekker, New York, 1980.
44 H. H. Yang, *Aromatic High-Strength Fibers*, Wiley, New York, 1989, p. 66.
45 S. Shabbir, S. Zulfiqar, S. I. Shah, Z. Ahmad and M. I. Sarwar, *J. Phys. Chem. B*, 2010, **114**, 13241–13248.
46 S. Zulfiqar, Z. Ahmad and M. I. Sarwar, *Aust. J. Chem.*, 2009, **62**, 441–447.
47 S. Zulfiqar, F. Karadas, J. Park, E. Deniz, G. D. Stucky, Y. Jung, M. Atilhan and C. T. Yavuz, *Energy Environ. Sci.*, 2011, **4**, 4528–4531.
48 Q. A. Wang, J. Z. Luo, Z. Y. Zhong and A. Borgna, *Energy Environ. Sci.*, 2011, **4**, 42–55.
49 L. Zhao, Z. Bacsik, N. Hedin, W. Wei, Y. H. Sun, M. Antonietti and M. M. Titirici, *ChemSusChem*, 2010, **3**, 840–845.
50 P. Galhotra, J. G. Navea, S. C. Larsen and V. H. Grassian, *Energy Environ. Sci.*, 2009, **2**, 401–409.
51 F. Karadas, C. T. Yavuz, S. Zulfiqar, S. Aparicio, G. D. Stucky and M. Atilhan, *Langmuir*, 2011, **27**, 10642–10647.
52 U.S. Department of Commerce, *NIST Reference Fluid Thermodynamic and Transport Properties Database (REFPROP)*, http://www.nist.gov/srd/nist23.cfm, accessed July 2011.
53 S. Zulfiqar and M. I. Sarwar, *Adv. Polym. Technol.*, 2010, **29**, 300–308.
54 S. Zulfiqar and M. I. Sarwar, *High Perform. Polym.*, 2009, **21**, 3–15.
55 S. Zulfiqar and M. I. Sarwar, *Nanoscale Res. Lett.*, 2009, **4**, 391–399.
56 H. A. Patel, F. Karadas, A. Canlier, J. Park, E. Deniz, Y. Jung, M. Atilhan and C. T. Yavuz, *J. Mater. Chem.*, 2012, **22**, 8431–8437.
57 D. M. Ruthven, *Principles of Adsorption and Adsorption Processes*, John Wiley & Sons, Inc, New York, 1984.
58 K. S. W. Singh, D. H. Everett, R. A. W. Haul, L. Moscou, R. A. Pierotti, J. Rouquerol and T. Siemieniewska, *Pure Appl. Chem.*, 1985, **57**, 603–619.
59 H. A. Patel, F. Karadas, J. Byun, J. Park, E. Deniz, A. Canlier, Y. Jung, M. Atilhan and C. T. Yavuz, *Adv. Funct. Mater.*, 2013, **23**, 2270.